J Electroceram (2007) 19:95–110
DOI 10.1007/s10832-007-9040-7

Thick-film piezoceramics and devices

R. N. Torah · S. P. Beeby · M. J. Tudor · N. M. White

Received: 30 May 2006 / Accepted: 11 October 2006 / Published online: 24 February 2007

Abstract Over the past 20 years, thick-film (screen printed) technology has been shown to possess a variety of desirable characteristics, which are particularly suitable for the realisation of micro-sensors and actuators. In particular, thick-film sensors are noted for their robust, versatile, compact and inexpensive nature. This paper will describe how screen printed thick-films can be used as the basis for a variety of piezoelectric a transducers. It will be shown how the technology can be combined with MicroElectroMechanical Systems (MEMS) to generate new types of micro-engineered structure. The evolution of the technology to a successful enabling mechanism for modern-day solid state sensors is described. The paper begins with a brief overview of piezoelectric thick-films including a discussion of the main factors relating to paste formulation, characterisation and techniques for fabricating devices. There is also a description of methods for fabricating thick-films on silicon, which opens up the possibility of using thick-film technology in the field of MEMS. A number of specific sensors and actuators are described, including accelerometers, micro-pumps, ultrasonic motors, slip sensors for prosthetic hands, resonators, elastic wave sensors and ultrasonic separators.

Keywords PZT · Thick-film · Screen-printing

1 Introduction and history

Advances in microsensor technologies have been largely driven by the developments in the field of microelectronics. Thick-film technology has been around for the last four decades and was originally developed for producing hybrid circuits, which combined monolithic silicon chips, thin-films and discrete components together with the thick-films themselves. The technology has also been successfully applied to the fabrication of a variety of sensors [1, 2] over the past 20 years or so.

The piezoelectric constant d_{33} is an important parameter for sensor and actuator applications as it relates the electrical charge produced for a given applied mechanical stress. Hence, this gives an indication of the sensitivity of the film. This property is particularly significant because the majority of applications using planar technology have electrodes on the upper and lower surfaces of the film and thus the poling field and measurement direction are both in the '3' axis.

One of the issues not discussed in some of the early papers, is the problem associated with taking a measurement of d_{33} on a substrate. Flexural bending within the substrate can give rise to an incorrect measurement of d_{33}. This point is addressed in Section 2.

There are many different piezoelectric materials, e.g. Quartz, Barium Titanate, Lithium Niobate, and Lead titanate. However, the most commonly used piezoceramic is Lead Zirconate Titanate (PZT).

Piezoelectric thick-films were first described by Baudry [3] in 1987, who fabricated an acoustic coupler to demonstrate an application of the technology. The thick-film material was based on a combination of lead zirconate titanate (PZT) powder, a small amount of glass frit and an organic vehicle. Finite element analysis was performed on various geometries of alumina substrate in order to find the optimum dimensions for thick-film piezoelectric buzzers. A further application addressed the design of an acoustic coupler.

Morten et al. [4, 5] (1989 and 1991, respectively) at the University of Modena, Italy, describe how piezoelectric

R. N. Torah · S. P. Beeby · M. J. Tudor · N. M. White (✉)
School of Electronics and Computer Science,
University of Southampton, Southampton SO17 1BJ, UK
e-mail: nmw@ecs.soton.ac.uk

thick-films based on PZT can be prepared and characterised. The quantity of glass binder in the formulation was varied from 3 to 30% by weight and it was found that the lower the glass content, the higher the value of d_{33}. The authors also suggest that the d_{33} coefficients of pastes prepared with a lead oxide binder were greater than those measured on similar pastes using lead-alumina-silicate glass.

A study undertaken by Moilanen et al. in 1993 investigated several ways to reduce the number of print cycles required for the fabrication of multilayer actuators. A novel screen-printing technique, known as double-paste printing, was developed for this purpose [6]. The technique maximises the efficiency of the printing process as it only requires a single screen to be aligned. The method will not work for all types of transducer design, but it is suggested to be particularly beneficial for reducing costs in the mass production of multilayer stacked actuators.

2 Characterisation

As previously described, the piezoelectric charge constant, d_{33}, is often used as the defining piezoelectric characteristic for improvements in piezoceramic technology. The most common technique for measuring d_{33} is the so-called *direct* or *Berlincourt* method, applying a force to the piezoceramic and measuring the charge generated. Thick-film technology requires the piezoelectric layer to be printed on a substrate. Therefore, care must be taken when using the direct method with thick-film samples as the substrate can bend during the measurement and lead to inaccurate readings. The Take-Control PM35 piezometer [8] is an example of a commercial instrument designed to measure d_{33} values in bulk piezoelectrics. This has been shown to produce consistent values of d_{33} provided that allowance is made for the effect of bending stresses within the substrate and the sample is held firmly in the rig. By altering the substrate supporting structure it has been shown that a Berlincourt method based piezometer can also be used to measure e_{31} (and therefore d_{31}) [9]. The sample is supported by a ring structure whilst the upper force is applied on the sample surface at the centre of the ring. The analysis requires some basic mathematical treatment which is presented in [9].

Work carried out by Dorey and Whatmore on sol-gel thick films also explored the effect of substrate clamping on the measured d_{33} [10]. The substrate clamping effect introduces stresses in the PZT film which distort the unit cell and reduce the effectiveness of the polarisation process.

Torah et al. [17] suggests that the effect of clamping reduces the measured piezoelectric coefficient of the film. The reduction is due to the effect of the d_{31} coefficient. Theoretical analysis predicts a reduction in the measured d_{33} of 62%. This result is obtained using Eq. 1 with values for d_{33} and d_{31} taken from standard commercial PZT-5H products. The full analysis for Eq. 1 is given in [17].

$$\left(\frac{D_3}{T_3}\right)_E = d_{33,f} = d_{33} + 2d_{31}\left(\frac{-\left(\frac{v_{\text{sub}}}{Y_{\text{sub}}}\right) - s_{13}^E}{\left(s_{11}^E + s_{12}^E\right)}\right) \quad (1)$$

PZT-5H thick-films from the study have a measured, clamped d_{33} value of 130 pC/N, which is therefore the equivalent of an unconstrained value of around 350 pC/N.

It is important to recognise the significance of the clamping effect when quoting measured piezoelectric quantities. Therefore, it is typical to quote the piezoelectric constant for thick-films as $d_{33,\text{f}}$ to signify it is a film and not a bulk piezoceramic.

3 Formulation

A PZT thick-film will typically begin as a thixotropic paste which enables the paste to pass through the screen easily but retain its subsequent printed geometry. The paste will consist of the active piezoelectric material, a suitable ceramic binding agent, such as lead borosilicate glass, and an organic vehicle to ensure the paste is thixotropic and therefore suitable for deposition. The percentages of these ingredients will be application and process specific.

Morten et al. [4, 5] describe the preparation and characterisation of piezoelectric thick-films based on PZT. The quantity of glass binder in the formulation was varied from 3 to 30% and it was found that the lower the glass content, the higher the value of d_{33}. The authors also suggest that the d_{33} coefficients of pastes prepared with a lead oxide binder were higher than those measured on similar pastes using lead-alumina-silicate glass.

Work by Torah et al. [11] has emphasised the significance of the formulation of the paste on the piezoelectric properties of the ceramic films. The studies have shown that the milling process required to produce the PZT powder can determine the homogeneity of the paste and therefore the consistency of the thick-film prints. Ball, Attritor and Jet milling of PZT powders were evaluated. Ball milling produces smooth, rounded particles with a reasonably tight particle size distribution. Attritor milling is used to further tighten the particle size distribution and produce a more uniform particle size in the powder. Jet milling is a more abrasive process and produces irregular shaped particles in a wider size distribution than ball milling.

The study revealed that the larger particle size of the ball milled powders produced the highest piezoelectric activity but that the tighter particle size distribution of the attritor

milled powders produced the most consistent results. Following these results, further studies investigated the combination of ball and attritor particles to improve the density of the films [12]. The results showed that a combination of 18% Attritor and 72% Ball milled PZT powders, with 10% lead borosilicate glass by weight produced the optimum paste composition. Combining this result with a peak firing temperature of 1,000 °C and a poling temperature of 200 °C produced a measured $d_{33,f}$ value of 131 pC/N.

Investigations concerning the use of dispersants in PZT films as a means of optimising the particle distribution have also been conducted. In order to improve the quality of the printed films it is essential that the paste spreads evenly on the substrate. Dispersants act to create repulsive forces between the particles, thus reducing clumping and increasing the homogeneity of the film. Thiele and Setter [7] have studied various dispersants and their effects on the rheology of thick-film pastes. Their experiments looked at eight commercially available dispersants with a Sensor Technology BM500 PZT powder. The results showed that a phosphate ester oligomer was the optimum dispersant. Rheological and optical microscopy measurements of the fired film surfaces highlighted the benefits of using a dispersant in the thick-film paste formulations. A decrease of 40% in mean surface roughness was observed for the film containing the dispersant compared with the sample containing none. The addition of only 0.1 wt.% of the dispersant resulted in a dramatic decrease in viscosity (2.42–0.22 Pa.s), which allows for a higher concentration of solids. They also showed that the dispersant has no adverse effects upon the dielectric and piezoelectric properties.

4 Polymers

Interesting developments in polymer materials have recently led to their increasing use in thick-film devices [13, 14]. Polymer devices have the advantage of having simple fabrication techniques, low cost and most significantly, the ability to be deposited on a wider range of substrates. The methods of depositing polymer films can include; spinning or casting, screen printing, electrochemical polymerisation and vacuum deposition.

The most common piezoelectric polymer in sensor and actuator applications is polyvinylidene fluoride (PVDF) [15]. The devices using piezoelectric polymers are similar to standard cermet films but with greater flexibility in design and processing. The films can be cured at lower temperatures (100–250 °C) and poled at lower voltages in comparison to standard cermet films. This enables these films to be compatible with plastic substrates as well as other materials with low resistance or melting points. Current PVDF films have low Curie temperatures of around 80 °C and comparatively low piezoelectric constants, with a measured $d_{33,f}$ of 24 pC/N [15].

Studies by Papakostas et al. [16] have considered the use of polymer binders in thick-film pastes. This replaces the standard glass frit binding material in an effort to lower the processing temperatures. The experiments used PZT5H powder and Ronascreen Green OPSR 500 polymer. Three pastes were analysed in 90, 85 and 75 wt.% PZT powder concentrations with their respective amounts of polymer paste. These pastes were printed on to an alumina substrate with a capacitor structure of two electrode layers with the test paste in between. The bottom electrode was a standard cermet silver/palladium ESL 9635-A paste used for convenience in the experiment. The top electrode was a standard silver polymer ESL 1107-S paste.

The PZT/Polymer layer was printed and then dried in an IR drier at 140 °C for 10 min; this partially cures the polymer. The samples were cured under a polarising field for 1 h, with a selection of samples poled for 24 h. Poling/Curing was conducted at 130 °C with an applied field of 3 MV/m.

The results showed the 85 wt.% concentration to give the best results, with a $d_{33,f}$ of 15 pC/N. The results also indicated that the poling time does not result in a significant improvement in $d_{33,f}$ and this allows for poling to be concurrent with curing. This is a low figure for $d_{33,f}$ and the measurement method used is not very accurate. The low $d_{33,f}$ value is thought to be influenced by the lack of a high temperature firing process for the PZT powder, thus the stoichiometry of the material remains in the pre-fired state and not at the morphotropic phase boundary where the optimum piezoelectric properties occur.

5 Substrates

Unlike bulk ceramics, thick-film materials are deposited on to a substrate to provide structural integrity to the films as they are dried and fired. The substrate is therefore an essential component of the thick-film process. The majority of thick-film applications incorporate the substrate into the overall device structure. Therefore, the substrate material becomes a critical component in any sensor or actuator design.

5.1 Alumina substrate

Many PZT thick-film devices use alumina substrates since they are inexpensive and offer good adhesion for the printed layers whilst being sufficiently rigid to reduce the influence of substrate bending moments on the device [17]. Alumina is hermetic so moisture is not able to seep in and reduce the quality of the prints during firing. In addition,

alumina has a thermal expansion coefficient that is closely matched to most thick-film inks.

5.2 Silicon substrates

Printing thick-film sensors directly on to silicon substrates allows for the integration of sensors and electronics on to the same chip. In addition, the dimensional control achievable with micromachining and excellent mechanical properties of silicon increase the diversity of thick-film PZT/MEMS applications including resonators, accelerometers and micro-pumps [18–20]. However, lead diffusion from the thick-film layers into the silicon substrate during firing is a significant problem for MEMS applications. Work by Maas et al. has evaluated the use of a screen-printed Heraeus IP211 barrier layer [21]. The results showed that there was no lead diffusion into the substrate and that the lead diffusion into the barrier layer did not change its insulating characteristics. The authors therefore concluded that further thick-film layers could be printed on to the barrier layer without short-circuits. This result is significant because one of the major limiting factors of using silicon substrates is the reaction caused by lead diffusion from the PZT film. A reduction in this lead diffusion enables further micro machining of the silicon substrate and the full integration of sensor and electronics.

An alternative to barrier layers is to reduce the maximum firing temperature for the thick-film layers. This has the effect of reducing the amount of lead diffusion. Chen et al. developed an ultrasonic transducer consisting of a PZT film printed on to a silicon micro-machined system [22]. The films that were produced were screen-printed using Ultrasonic Powders Inc. PZT501A material with a 4 wt.% glass frit content, fired at 850 °C ensured no blistering of the bottom electrode. However, SEM micrographs showed the low firing temperature resulted in the presence of residual porosity in the films. This work showed that it was possible to print crack free PZT films onto silicon substrates; measurements showed that a maximum $d_{33,f}$ of 50 pC/N for the films was obtained. The effect of firing temperature on lead migration in silicon is discussed further in Section 6.3.

5.3 Glass substrate

Studies by Kohler et al. have highlighted the future possibilities for glass as a substrate [23] for use in optoelectronic circuits such as optocouplers or isolation amplifiers. These studies involved polymer-based thick-film conductors and resistors due to the limits of low temperature firing with a glass substrate. The study has shown that hybrid thick-film circuits are a viable area for development, with future possibilities for piezoelectric thick-films being incorporated into optoelectronic systems. The precise actuation control that can be achieved with thick-film actuators makes them ideal for micro-mirror movement and other optoelectronic switching systems.

5.4 Steel substrate

Thick-film piezoceramics have been successfully screen printed onto metallic substrates most notably for the fabrication of a piezoelectric vibration energy harvesting device [24, 25] and triple beam tuning fork resonators [26]. Only certain types of steel are suitable due to the high firing temperature which results in excessive carbonisation of the majority of materials. The types of stainless steel that are suitable include AISI AISI 304, AISI 430S17 and AISI 316. Thick-film ink manufacturers have developed a range of dielectric and conductive inks designed to for these materials. For example the ESL 4924 dielectric is intended for use with 430S17 and Heraeus IP222 has been successfully used with type 316. The steels are available in sheet form in a wide range of thicknesses and can be chemically etched with a photolithographic patterning process to define mechanical structures.

6 Fabrication

Thick-films are deposited by a screen-printing process. Screen-printing is an attractive process in MEMS applications because it is possible to batch print diverse patterns on a variety of substrate materials. Screen-printing therefore opens a broader range of possible applications than the traditional construction techniques such as pressing and extrusion [27]. The process is suitable for mass production and offers the ability to produce films of thickness 10–100 μm in a single print stroke.

6.1 Screen-printing process

Figure 1 shows the four stages of the screen-printing process. The ink is spread across the screen by a flood blade ready for printing (a). A polyurethane squeegee then forces the screen down on to the substrate as it begins the print stroke (b). The squeegee is then drawn across the screen, forcing the ink through the etched sections of the mask and removing the excess ink (c). Finally, at the end of the print stroke, the pressure of the squeegee is removed and the screen springs back into the start position leaving the ink deposited on the substrate in the desired pattern (d).

The printing process allows a number of layers to be printed in sequence on top of the previous layers. The printing pressure and the gap between the screen and the

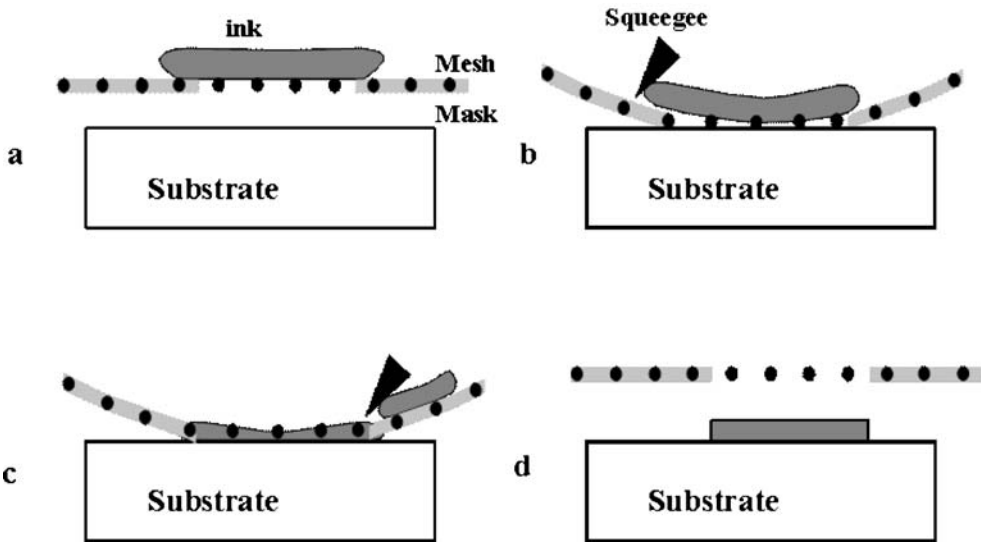

Fig. 1 Process steps for screen-printing

substrate control the thickness of the printed layer. Therefore, for subsequent printed layers it is necessary to increase the gap size to ensure the screen can spring back without smearing the print.

Limitations of conventional screen-printing are the minimum feature size and geometry achievable; typical minimum line width and space being 100–150 microns. Addressing this issue, Robertson et al. have developed a thin stainless steel foil into which the required pattern is etched called the μ-Screen [28]. This custom etched mesh is mounted in a conventional screen frame and is therefore compatible with standard printers. This also alleviates any potential problems with screen flexibility. The μ-Screen provides a higher resolution, 50 μm line width, and better edge definition than current fine line technology. The technology is not limited to squared off designs, curved lines and circular pads can also be produced easily on the mesh. Figure 2 shows a close up of the underside of an etched foil screen.

6.2 The sol-gel process

In general, thick-films are defined as films of 10–200 μm. The Sol-Gel technique is usually known as a thin film technique but has seen increasing applications in thick-film devices [29]. Sol-Gel involves the transition of a mainly non-crystalline liquid solution, the sol, into a solid phase, the gel. Preparation of the sol involves the use of inorganic metal salts or metal organic components. The sol can then be processed further to make ceramic materials in various forms. This typically involves the formation of thin-films on a substrate by spin or dip coating and subsequent drying and firing.

Work by Kim et al. [30] has seen the development of a composite technique for increasing the piezoelectric activity of a screen-printed PZT thick-film. A PZT paste was screen-printed on to a silicon substrate leading to a final film thickness of 20–40 μm. A number of drying and burn-out stages were used to remove the organic binder from the film. Subsequently, a Sol-Gel PZT solution was applied to the dried thick-film PZT layer. The composite film was then sintered using temperatures of 700, 800 and 900 °C to observe the effects of firing temperature on the film and substrate. SEM micrographs of the films show that the sol-gel treatment improved the density of the films although they were still porous. The 800 °C firing profile produced the optimum results, the measured $d_{33,f}$ value was increased from around 75 to 177–200 pC/N with the application of a Sol.

A similar development by Corker et al. [31] has seen the fabrication of thick-films using a composite of a ferroelectric powder and an organo-metallic sol. The solution was made using a Ferro Pz26 PZT powder mixed with the sol, a Kenrich KR55 dispersant and 5 wt.% liquid phase sintering aid. The film was deposited onto Kovar and platinised

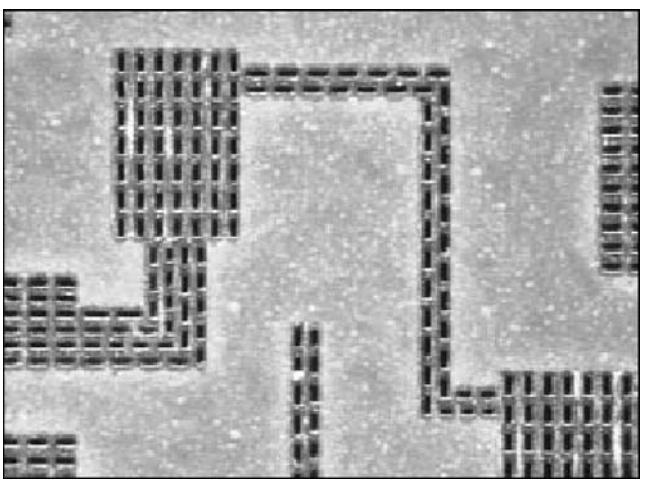

Fig. 2 Close up of the underside of an etched foil screen. *Holes* are etched only where printing is required (after Robertson et al. [28])

silicon substrates using spin coating. The films were dried on a hotplate at 450 °C for 15 s. This process was repeated to build up a composite layer thickness between 8 and 40 μm. The films were fired at 710 °C for 30–45 min in an argon atmosphere. After firing, the films were polarised and subsequent measurements revealed $d_{33,f}$ values of 50 pC/N. The results showed that the film density was higher than that achieved with conventional thick-films. It was noted, however, that the films are denser close to the substrate than at the top of the film. This is considered to be due to a number of factors. These include; the sintering aid sinking within the film, the organic vehicle burnout during sintering resulting in pores and a similar effect caused by lead evaporation during firing.

6.3 Firing process

PZT piezoceramics produce the optimum piezoelectric activity when the composition lies near the Morphotropic Phase Boundary (MPB) [32]. The MPB is a boundary that separates the tetragonal and rhombohedral ferroelectric phases. PZT compositions that lie on the MPB are said to have both of these phases coexisting, which allows for a greater number of polarisation directions and improved results from the polarisation process [33]. Commercially available PZT powders are formulated to provide the optimum stoichiometry once fired. This is typically based on the predicated phase change within the material during the firing process. Therefore, it is essential to match the firing process with the material being used to achieve the optimum piezoelectric activity.

For the production of glass-ceramic (cermet) piezoelectric films, it is necessary to sinter them at a suitable temperature (typically around 900 °C) to cause the binding material (a lead-based glass) to melt with the PZT powder and form a bonding matrix. The films form a fired, composite material, often having different electro-mechanical properties from those of the bulk material.

Studies by Glynne-Jones et al. have been conducted into the firing profile for thick-film layers on silicon [34]. The films were based on PZT type 5H supplied by Morgan Electro Ceramics Ltd., and were fired over a range of temperatures from 750–1,000 °C. The results showed that films at the lower firing temperature of 750 °C exhibited poor sintering. At temperatures above 800 °C, samples showed acceptable adhesion and sintering. The samples fired at the lower temperature exhibited d_{33} values of between 101 and 109 pC/N. A maximum value of 169 pC/N was obtained from the samples fired at 1,000 °C. This is due to the improved sintering of the film at these higher temperatures. One drawback, however, is that the increased firing temperature causes lead to migrate from the film and pollute the surface of the silicon.

7 Silicon processes (MEMS)

The combination of the screen printing process with silicon micromachining is, perhaps, not an obvious choice. The screen printing process is a physical process that exerts pressure on the substrate. Micromachined silicon devices typically have sub-micron feature sizes and are too fragile to withstand the printing process. In addition, the resolution and accuracy of alignment registration is generally poorer than that achievable with photolithographic processes. There is, however, certainly a place for micromachined silicon devices incorporating thick-film piezoelectric films. Micropumps are an example of a larger device that requires more substantial actuating forces than those achievable with typical thin-film piezoelectric layers. Other advantages include the fact the screen printing process deposits the material in the desired pattern, thus negating the need for subsequent photolithographic and etching steps. The screen printing process is essentially a simple, batch compatible low-cost process, which is accessible to a wide range of MEMS developers. Combining screen printable piezoelectric layers with micromachined structures opens up a large number of opportunities for various sensing and actuating applications.

The first published research into PZT films on silicon by Chen et al. and further developments by Maas et al. were covered in Section 5.2. The combination of screen printed piezoelectric films and micromachined silicon structures was explored further by Beeby et al. [35, 36]. This work investigated the spread of the reaction caused by the lead evaporation versus firing temperature. The investigation confirmed that the reaction begins at a temperature of 850 °C and continues as the temperature increases. The reaction process has also been studied by Thiele et al. who have postulated that the reaction product is a lead silicate [37]. In contrast to the findings of Mass, Thiele found the reaction material to be non-conducting. Thiele also reported evidence of the diffusion of silicon ions into the film at high firing temperatures. This diffusion results in the formation of zircon crystals ($ZrSiO_4$) in PZT films fired at 950 °C for 1 h, and reduces the dielectric properties of the PZT film.

Thiele's work also explored the possibilities of performing standard micromachining processes on wafers with thick-film piezoelectric films already deposited. The wafers were exposed to a variety of photolithographic and wet and dry etching processes. In summary, the plasma based dry etch processes were found not to affect the PZT or electrode films. The lower platinum electrode could therefore be used as a masking layer for subsequent silicon etches. This development led to the definition of a process whereby structures could be defined and released after printing of the PZT and top electrode films (see Fig. 3). The lead migration reaction product, however, was found to inhibit these etches and

could potentially cause difficulties in accurately defining structures. Some of the devices discussed in the following sections have been fabricated using this process.

8 Devices

Thick-film piezoelectric devices have been used in a variety of applications. In the first paper on thick-film piezoelectrics, published in 1987, Baudry [3] describes the design of two devices. The first is a thick-film piezoelectric buzzer. These have the advantages of light weight, low power consumption and robustness. The second application was that of an acoustic coupler. Such devices can be used as a means of communicating across an electrically insulating region. Two piezoelectric layers were fabricated onto both sides of an alumina substrate so that they were mechanically bound but electrically isolated. The frequency of operation was designed to be 100 kHz, well beyond the audible range.

8.1 Micropumps

An early example of combining screen printed thick-film PZT layers with silicon micromachined structures is described by Koch et al. [38, 39]. A micropump was fabricated comprising three silicon wafers that were fusion bonded together. The device is depicted in Fig. 4.

The passive cantilever valves were produced by a boron etch stop technique and fusion bonding. Tests of the valves showed good performance, as no flow could be detected in the reverse direction. Initial experiments on a thick-film screen printed piezoelectric membrane actuator were undertaken. A study of suitable pastes for electrodes on different insulation layers on silicon revealed silicon dioxide and cermet gold paste as the most satisfactory combination. Deflection measurements of a 7×3 mm PZT and 8×4 mm silicon bimorph membrane gave 1 μm movement at an applied voltage of 100 V. A quasi-static simulation package of the flow through the micropump was also undertaken. The valve action was simulated using the ANSYS finite element package coupled with FLOW3D. Pump rates of up to 400 μl/min with a maximum backpressure of up to 35 kPa at 100 V driving voltage across the PZT were measured. The existence of lead pollution around the area of the PZT was noted and this had the effect of causing the SiO_2 barrier layer to become conductive as mentioned previously.

A further example of this design has been developed for a drug delivery system by Junwu et al. [40]. With a valve length of 2.5 mm they have achieved maximum flow rates of 3.5 ml/min and a backpressure of 27 kPa. Their system is designed to work at two frequencies, 0.8 and 3 kHz, which enables precision control of the dosage amount at the higher frequency but maintaining the speed and volume of delivery at the lower frequency.

A similar diffuser micropump has been developed by Kim et al. [41] and uses a TMAH-etched diaphragm with a screen printed PZT-PCW actuator on rectangular or square diaphragms of approximately 20 microns thickness (see Fig. 5). A lead-based complex oxide (PCW) additive has been infiltrated into the screen printed PZT film to improve both density and the electrical properties. The pump chamber was etched into either a Pyrex or silicon wafer, which is bonded to the actuator wafer to form the sealed cavity. The resonant frequency of a typical pump design is 53.3 kHz in air and this falls to 32.4 kHz when filled with a fluid. The overall size of the pump is 9×11 mm in size and the optimum geometry of PZT (1.5×1.5 mm) produces a mean flow rate of 5.3 μl/min.

8.2 Accelerometers

Several different configurations of piezoelectric thick-film accelerometer have been documented. Crescini et al. have developed a thermally compensated thick-film accelerometer [42]. The device uses two sensing elements, printed on either side of the substrate in a planar capacitor structure, which allows for the reduction in thermal drift. By connecting the two piezoelectric elements in series and packaging the sensing elements and electronics close together, it is possible to reduce the effects of the extra charge generated with increase in temperature. This, however, requires that the manufacturing tolerances of the devices are extremely close together. The two devices are polarised in the same axis, but have opposite polarity. This

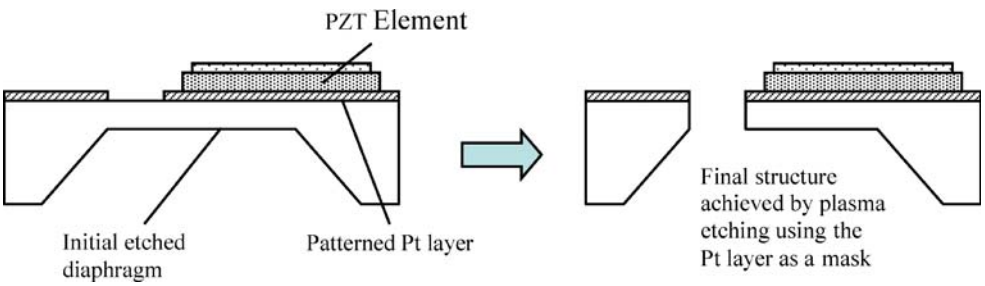

Fig. 3 Combined silicon micromachining and thick-film piezoelectric fabrication process

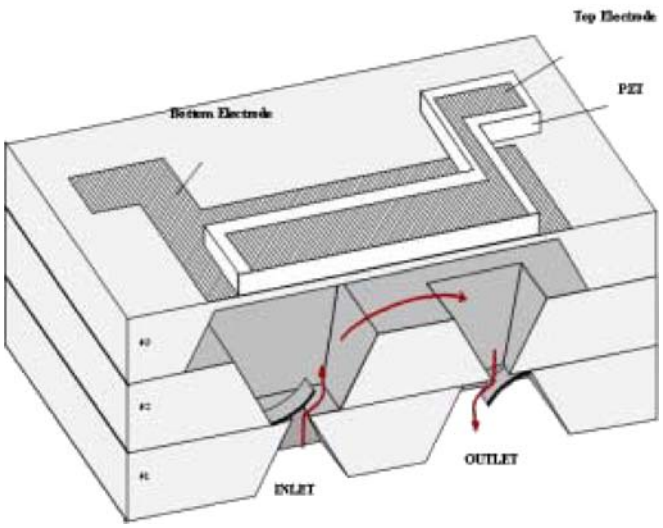

Fig. 4 Combined silicon/thick-film micropump (after Koch et al. [38])

means that thermal drift in one device will be the opposite polarity in the other and the effect is therefore nulled.

Figure 6 shows a schematic of the device. The high frequency cut-off is determined only by the resonance properties of the alumina substrate, the elastic properties of the case and the bonding techniques used. The printed films were 40–50 μm thick, with a d_{33} coefficient of around 180 pC/N, when poled at 3 MV/m.

Another example of a combined thick-film and silicon micromachined structure is the accelerometer described by Beeby et al. [43]. The device is a deflection-based dynamic mechanical accelerometer having a 17 mg inertial mass suspended by four silicon beams, each located at a corner of the seismic mass. The deflection of the inertial mass due to an applied acceleration is sensed using thick-film piezoelectric elements located on the supporting beams. Each piezoelectric element is printed as a planar capacitor structure with the active layer being sandwiched between an upper and lower electrode. As the mass moves relative to the chip frame, the beams deflect causing the piezoelectric layer to deform and hence a charge is induced. The amount of charge generated depends upon the piezoelectric properties of the printed layer and is proportional to the deflection generated by applied accelerations. The device is depicted in Fig. 7, which shows a finite element model of the device, together with a scanning electron micrograph of the actual device.

The total capacitance of the elements in this arrangement was measured at 360 pF. The accelerometer was tested on a Goodmans vibration generator type V50 Mk1. This was driven via a Goodmans PA50 VA power amplifier by an HP 35660A dynamic signal analyser. The system was calibrated using a Bruel & Kjaer accelerometer type 4369 and the charge was measured using a Kistler 5001 charge amplifier in order to determine the fundamental sensitivity in terms of pC/g. The sensitivity of the device was found to be 16 pC/g in the z (vertical) direction. The x- and y-axis cross-sensitivity was measured at 0.64 pC/g for the accelerometer, which is equivalent to 4% of the full scale output. The overall fabrication process was relatively straightforward, providing a yield in excess of 95%, which is quite impressive for a micromachined device. Evidence of the lead pollution around the PZT, as described in Section 6.3, can be clearly seen in the electron micrograph of Fig. 7.

8.3 Ultrasonic motors

Ultrasonic motors are based or the principle of converting vibrations into rotary motion. They offer the advantage over electromagnetic motors of removing the need for wire-wound

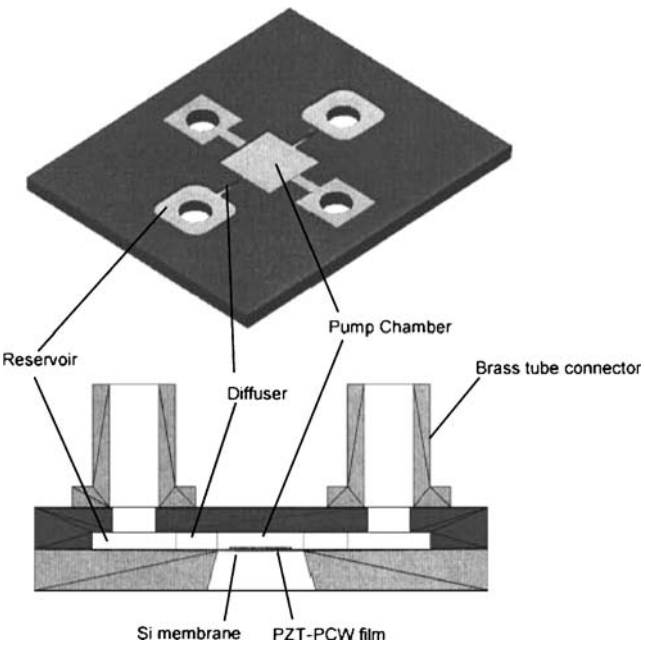

Fig. 5 Schematic of diffuser type micropump (after Kim et al. [41])

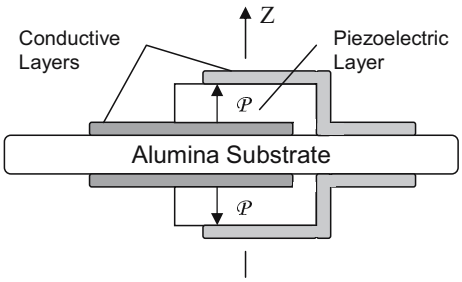

Fig. 6 Cross-sectional view of a thick-film accelerometer (after Crescini et al. [42])

components, such as the stator and rotor, and hence are amenable to integration using micro-fabrication techniques [44–46]. Aoyagi et al. [47] described an ultrasonic motor that uses thick-film PZT actuators to induce specific resonant modes into a substrate. These modes (B_{22}, B_{30} and B_{03}) are induced in different directions according to the electrode design. They can then be combined in order to vibrate the substrate. On the upper side of the substrate there is a ceramic column, which is moved as a result of the induced vibrations. A ball bearing, located on top of the column, has freedom of movement in all directions, and hence this type of motor is sometimes referred to as a multi-degree-of-freedom (MDOF) device. The principle of operation is illustrated in Fig. 8.

The stator of the ultrasonic motor consists of a 20 mm square alumina plate, 250 μm thick with an alumina cylinder, 3 mm outside diameter, 0.5 mm thick and 3 mm long, attached to the centre of the plate. This amplifies the lateral displacements of the plate associated with the bending modes, which on the surface of the plate, are relatively small. The alumina cylinder also holds a small ball bearing, which serves as the rotor at the centre of the vibrator. The thick-film PZT electrodes were printed on the underside of the alumina plate.

The arrangement of the thick-film electrodes and piezoelectric elements is shown in Fig. 9. The structure was analysed on a purpose-built optical fibre interferometer. The applied excitation voltage for these measurements was 200 V peak-to-peak. The resonant frequencies of the B_{30} and B_{22}-modes were found to be to 15.45 and 16.2 kHz, respectively. Finite element analysis had predicted that the resonance frequencies of the B_{30} (B_{03}) and B_{22} modes were 14.47 and 16.49 kHz, respectively. These frequencies should, ideally, be the same in order to reduce both the mechanical and, as a result, electrical impedance. The resonance responses were, however, rather small and this is because the thick-film printed PZT layer has a relatively low piezoelectric coefficient, d_{31}, of approximately −33 pC/N compared to the bulk value of −274 pC/N. Rotation angles of the rotor were changed by applying short bursts containing a number of sinusoidal pulses with a frequency of 16.23 kHz and an amplitude of 200 V peak-to-peak. Precision positioning of the rotor was found to be possible with this device and a resolution of rotor angle of approximately 0.08° per unit pulse after 5 ms burst of drive pulses is achievable.

8.4 Prosthetic hands—slip sensors

One of the problems with a majority of prosthetic devices is the lack of feedback control. In the case of a prosthetic hand, for example, the operator cannot feel an item within the grasp of the hand—the operator has no 'sense' of what it is that they are holding, beyond that being visually assessed. The inability to monitor the grip force imposed on a grasped item means that the user cannot be totally sure of the security of the grip and is unaware when the object begins to slip from their grasp.

An example of a prosthetic hand is shown in Fig. 10 [48]. This is a prototype myoelectrically driven device, which was designed at the University of Southampton. In use, the hand is controlled by the electrical signals produced by any convenient flexor-extensor muscle pair; one signal opens the hand and the other closes it. Each finger on the hand is individually controlled by its own

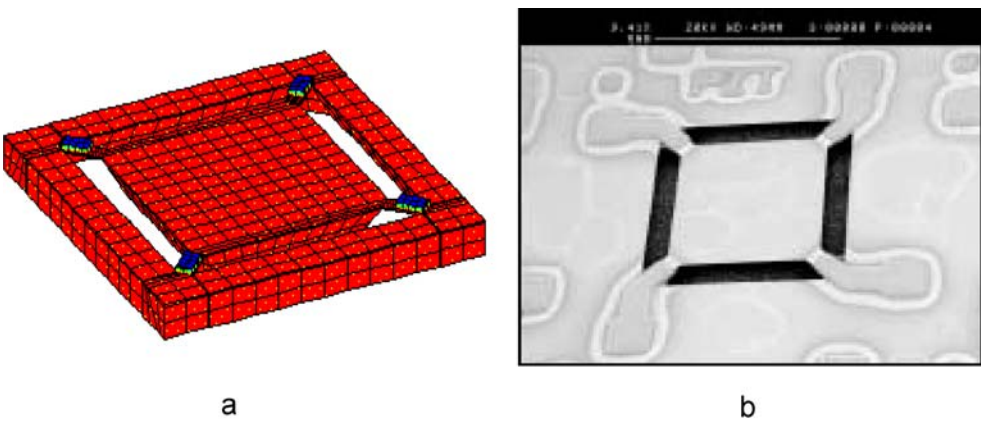

Fig. 7 **a** Finite element model and **b** electron micrograph of a combined thick-film/silicon accelerometer (after Beeby et al. [43])

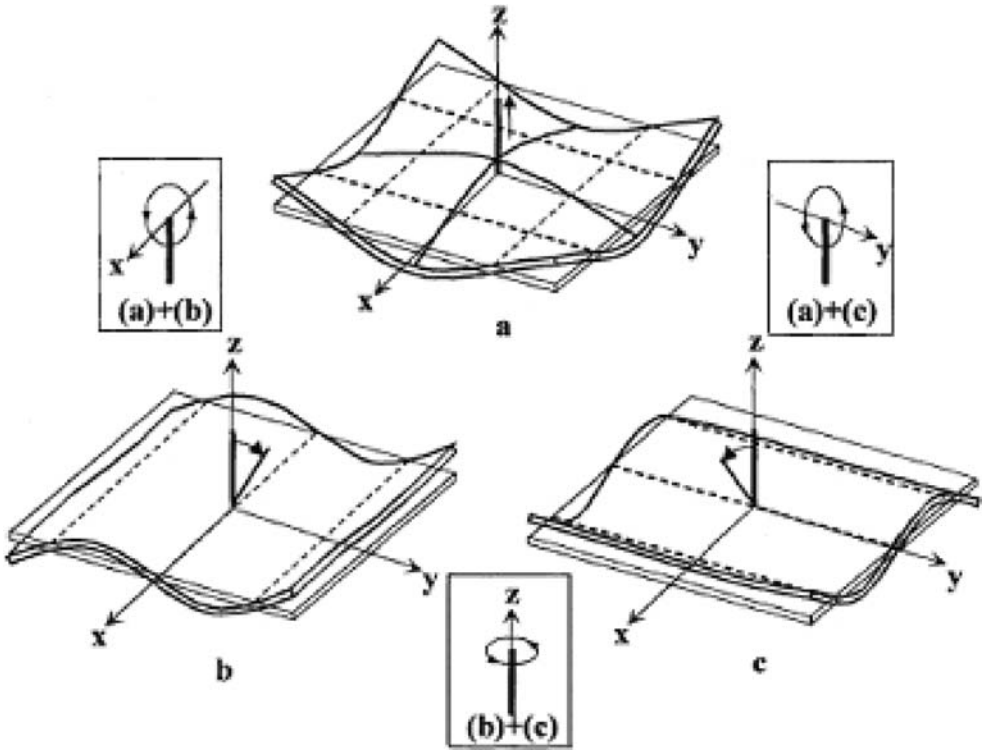

Fig. 8 Resonant modes in a multi-degree-of-freedom ultrasonic motor, B_{22}, B_{30} and B_{03}, respectively, and their associated displacements, (after Aoyagi et al. [47])

dedicated motor, allowing independent flexion and extension of each mechanical digit. Thick-film piezoelectric sensors have been fabricated onto the stainless steel finger tip as described by Cranny et al. [49], and shown in Fig. 11. These are primarily intended to act as slip sensors. If an object is being held within the hand, the PZT sensors can detect the onset of slip by detecting the vibrations within the finger tip. A signal can then be sent to the motors to cause the hand to grip tighter.

8.5 Resonators

Resonant sensors confer a number of benefits over those with traditional analogue outputs. They can be very sensitive and versatile, allowing the measurement of a variety of variables (pressure, acceleration, mass, viscosity, etc.). Also frequency can be a very convenient form of information encoding, as it permits the acquisition of data

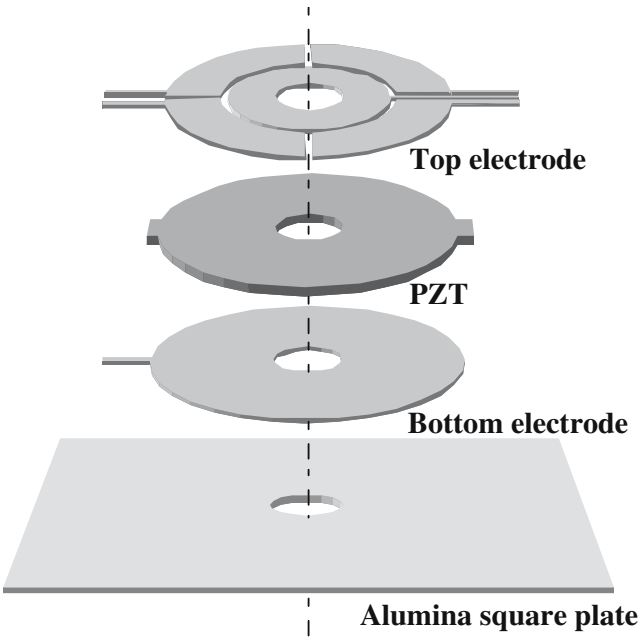

Fig. 9 A schematic of the arrangement of the PZT and electrode layers of the thick-film ultrasonic motor (after Aoyagi et al. [47])

Fig. 10 The Southampton-Remedi prosthetic hand (after Light and Chappell [48])

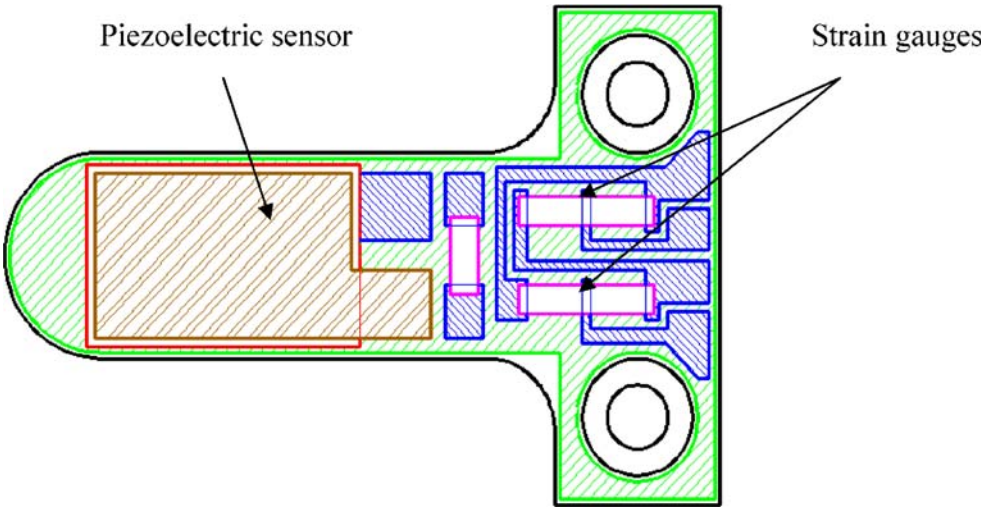

Fig. 11 Prosthetic hand finger-tip comprising piezoelectric slip sensor and thick-film strain gauges (after Cranny et al. [49])

via simple timer-counters such as those provided with modern microcontrollers. Yan et al. describe an application for thick-film piezoelectric materials as the excitation and detection mechanism of a triple beam resonator [26]. The device consists of three beams (or tines) aligned alongside each other and joined at a de-coupled region at each end to the surrounding material. The central beam has twice the width of the two outer beams. The resonating element has an overall length of 15.5 mm, a thickness of 0.25 mm and beam widths of 2 and 1 mm, respectively. The distance between the beams is 0.5 mm. A photograph of a sheet of devices is shown in Fig. 12.

Thick-film PZT elements were screen printed on separate regions at each end of the central beam, where maximum surface strains exist. The PZT element at one end acts as an actuator, driving the vibrations, whilst the other element detects them. Positioning the PZT driving and sensing elements on the regions of maximum stress, optimises the driving forces and sensing signals. The substrate of the resonator was etched from a 0.5 mm thick 430S17 stainless steel thin plate. A dielectric layer was screen printed, dried and fired at the defined driving and sensing regions on the top surface of the resonator using a standard screen-printing process. Consecutive layers of lower gold electrode, piezoelectric paste and upper gold electrode were then deposited and fired sequentially. The dielectric layer was required to isolate the lower electrode from the resonator substrate. The device is operated in its third mode of vibration, as this provides out-of-plane motion of the tines, whose moments of inertia cancel thereby providing a dynamically balanced structure with a quality factor, Q, in excess of 4,000.

Micromachined silicon beam resonators with thick-film piezoelectric drive and detection elements have also been

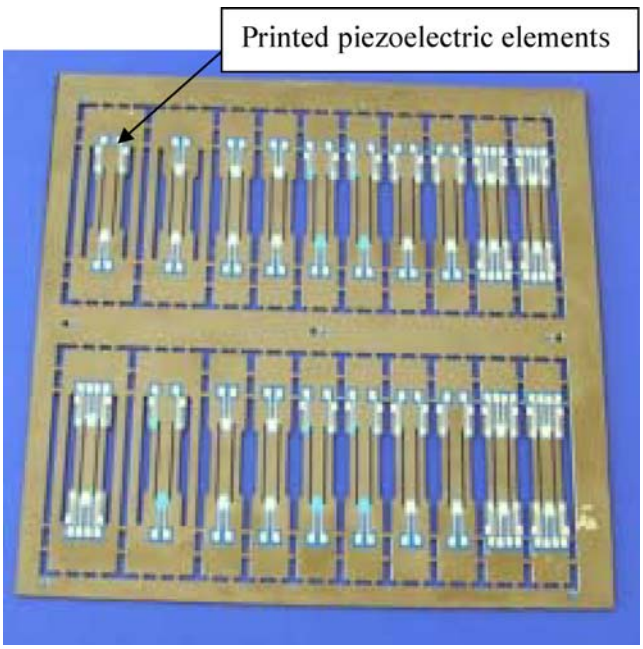

Fig. 12 A a sheet of triple-beam tuning fork resonator (after Yan et al. [26])

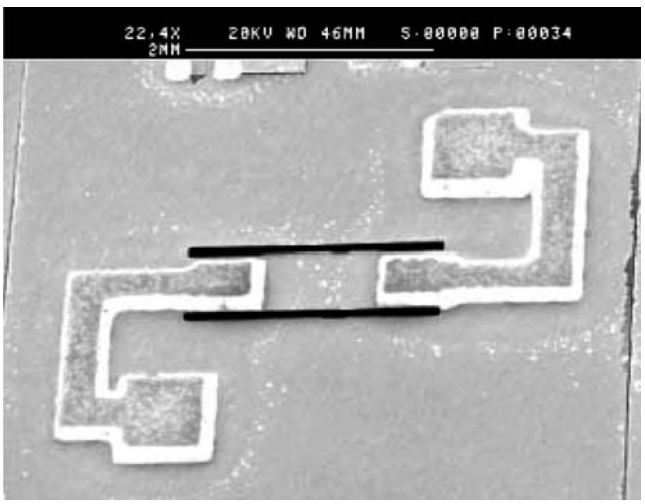

Fig. 13 Silicon encastre beam resonator with thick-film PZT drive and detection elements

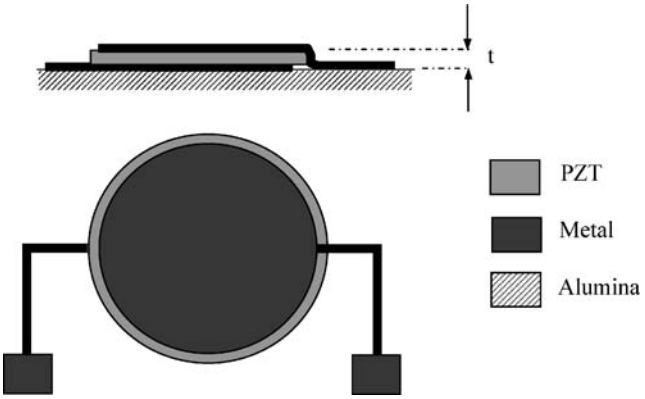

Fig. 14 Thickness mode piezoelectric thick-film gravimetric sensor (after Ferrari et al. [53])

demonstrated by Beeby et al. [50, 51]. The devices consisted of an encastre beam etched into a silicon membrane as shown in the SEM photo in Fig. 13. The fabrication process followed that described in Section 8 and depicted in Fig. 3. The screen printed PZT film of 40 μm thickness is sandwiched between a common evaporated Pt bottom electrode and a Au printed top electrode. Finite element analysis was used to simulate the device and this predicted a fundamental resonant frequency of 68.4 kHz which compared to the experimentally observed 56.5 kHz. The difference was predominantly due to the slight over-etching of the membrane producing a thinner than expected resonator. The *Q*-factor of this device was found to be 70 in air which highlights the increasing importance of gas damping effects on resonator structures as they reduce in size. It is also indicative of an unbalanced resonator structure, as opposed to the triple beam tuning fork discussed above.

The screen printed piezoelectric layer itself has also been used as a resonant structure. A planar capacitor structure, as shown in Fig. 14, printed onto an alumina substrate can be operated as a thickness mode resonant structure. When operated in such a mode, the structure is sensitive to mass loads applied on the free surface. Sensors have been fabricated by Ferrari et al. [52, 53] that demonstrate a mass sensitivity of 114 kHz mg^{-1} on devices with a thickness of 140–150 μm. Applications of such a structure include chemical sensing, whereby the thick-film structure is coated by a chemically sensitive material that adsorbs certain chemical molecules. The oscillator circuit that controls the resonance has been fabricated as a hybrid circuit around the sensor, demonstrating a compact solution readily achievable by exploiting thick-film sensor technology.

The PZT-PCW film used in the diffuser micropump discussed previously has also been employed in the fabrication of a resonant cantilever also designed as a mass sensitive resonator [54]. The cantilever is fabricated from silicon using a TMAH wet etch after which the PZT film is printed and the sol-gel solution infiltrated. Cantilevers from 850 to 2450 μm in length and 500 to 1100 μm in width were fabricated. The sensitivity of these cantilevers was determined by sputtering a gold film on the top surface. The short cantilevers proved to be the most sensitive with an additional 1 ng mass producing a change of a few 10 s of Hertz with a base resonance of 25 kHz. The intended application of this device is in biosensors where the cantilever would be used to detect minute changes in mass due to the adhesion of protein cells. The method of coating the cantilever with the protein sensitive film is, however, not discussed.

8.6 Elastic wave sensors

Piezoelectric thick-films have also been used as elastic wave sensors, in particular surface acoustic wave (SAW) devices [55–57]. An example, not drawn to scale, is shown in Fig. 15. The sensor comprises two interdigitated electrode patterns, screen printed and fired onto an alumina substrate of thickness 630 μm. The piezoelectric thick-film (thickness 40 μm) is deposited over the electrodes. The width and gap between the electrodes is 200 μm. The piezoceramic material is polarised between the 'fingers' of the electrode pattern.

One of the interdigitated transducers (IDTs) acts as an input device. A sinusoidal voltage is applied to the electrodes and, by virtue of the reverse piezoelectric effect, an elastic wave is generated within the film and travels

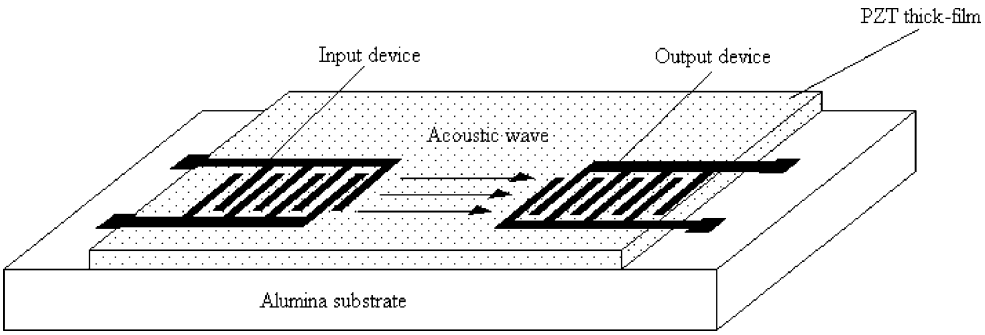

Fig. 15 A thick-film elastic wave sensor (after White and Ko [57])

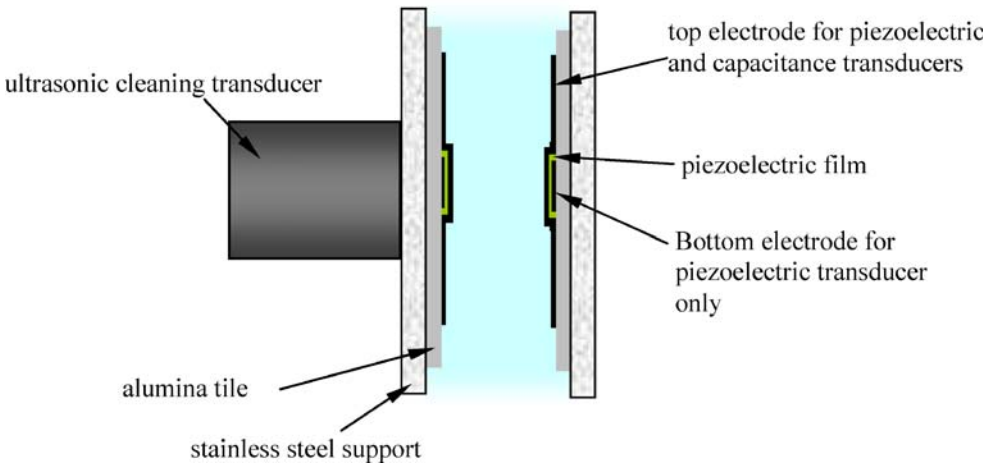

Fig. 16 A dual modality, thick-film sensor probe (after Hale et al. [58])

towards the other IDT. At the receiver, the acoustic wave is translated back into an electrical signal as a result of the direct piezoelectric effect. The wave velocity, ν, is determined by the acoustic properties of the medium. The wavelength, λ, is equal to the centre-to-centre distance between adjacent pairs of fingers. The frequency of the SAW device is therefore $F=\nu/\lambda$, and is typically around 5 MHz. Commercial SAWs have frequencies in the region 30 MHz–1 GHz. The device is usually operated as a delay-line oscillator by amplifying the signal from the output transducer and feeding back to the input. A phase shifter may also be required to ensure a total phase shift of a multiple of 2π around the loop. A number of mechanisms may be exploited in order to use the device as a sensor. The distance between the two IDTs is often referred to as the 'acoustic gap' and as the wave travels across this, an interfering medium such as a chemical, gas, biological or humidity sensitive coating will change a particular characteristic (amplitude, phase or frequency) of the wave. SAW sensors are therefore extremely versatile and find use in a wide variety of applications.

8.7 Multi-modal sensors

There is often a requirement to take multiple measurements in a given application. As an example, when crude oil is extracted from the ground, it is in a mixture containing water, gas and particulates. In order for the oil to be in a suitable state for refining, it needs to be separated from the mixture. This process is performed inside a separator vessel, which allows the mixture to settle into discrete phases. Typical operating conditions of such installations are characterised by high temperatures reaching in excess of 150 °C, pressures in excess of 150 bar, and the presence of aggressive chemical compounds. There are currently no commercial instruments that identify where the phase interfaces lie. This is partly because of the harsh environment, but also because the interfaces themselves are not clear. There is a gradual separation between the phases between the emulsion of oil and water and the foam of oil and gas. Hale et al. [58] and Dyakowski et al. [59] have considered the use of thick-film technology in solving this problem.

Figure 16 shows a schematic of the sensor probe, which contains thick-film capacitive and ultrasonic sensors together with a commercial, high power ultrasonic cleaning transducer. The capacitance sensors are used as part of a tomographic imaging system that distinguishes the various phases within the separator. The thick-film ultrasonic sensors are used to take a time-of-flight measurement across the fluid mixture and hence determine the velocity. The high power ultrasonic transducer, used for cleaning the sensor faces, is mounted on the back face of one of the stainless steel support plates. The ultrasound excites the adjacent sensor tile and couples into the process fluid, through which it propagates to the other sensor tile. This configuration allows both tiles to be cleaned using a single ultrasonic transducer. Owing to the relatively high operating temperature, PZT type 5A was used to fabricate the acoustic sensors. This material has a higher Curie temperature (350 °C) than type 5 H (180 °C).

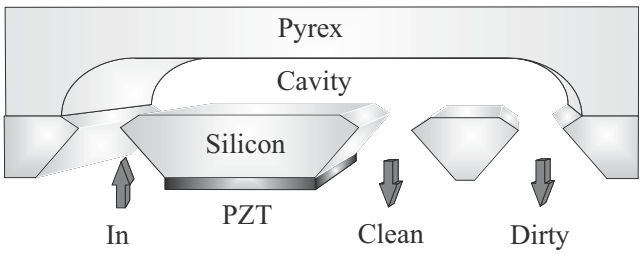

Fig. 17 Schematic cross-section of a microfluid separator (after Harris et al. [60])

Fig. 18 View of the outlets of the barrier-less filter with power off and power on, respectively (after Harris et al. [62])

9 Microfluidic separators

Ultrasonic standing waves can be used to generate small forces on particles within an acoustic field. This has the effect of moving the particles to a particular point within a fluid where the pressure forms a node or anti-node. The effect can be used to: aggregate particles in a specific area; manipulate and fractionate particular particles; or to separate groups of particles from the carrying fluid. Figure 17 shows a cross-sectional view of a micromachined device as described by Harris et al. [60–63].

The device uses a dual layer of co-fired PZT thick-film as the acoustic transducer, which is used to generate a standing wave field within the chamber. A fluid/particle mixture is drawn into the device through the port on the left of the figure. An acoustic standing wave, of a half wavelength, is maintained within the cavity and, as the particles move through the field, they migrate to the pressure node at the centre of the cavity. A fraction of the particle-free fluid can then be drawn from the 'clean' outlet and the remainder of the fluid/particle mixture can be drawn from the final ('dirty') outlet. Such a scheme allows for a relatively small quantity of clarified fluid to be produced, but different geometries have the potential to increase the proportion of recovered clarified fluid, or alternatively to increase the concentration of the particles recovered from the 'dirty' outlet. Tests have shown that this type of transducer is more efficient at converting electrical energy into acoustic energy than the traditional solution of bonding bulk PZT to the substrate. Efficiencies of 43% have been achieved, compared with, typically, 18% for bulk PZT having the same configuration.

The device has been manufactured in a combination of silicon and Pyrex. The latter, being transparent, allows visual inspection of the separation process. Figure 18 shows the device separating a continuous flow of water and yeast particles. Flow is from right to left and the view is looking down on the two outlets. The outlet at the far left of each picture is the outlet for the 'clean' flow and the outlet in the centre of each picture is the outlet for the 'dirty' flow.

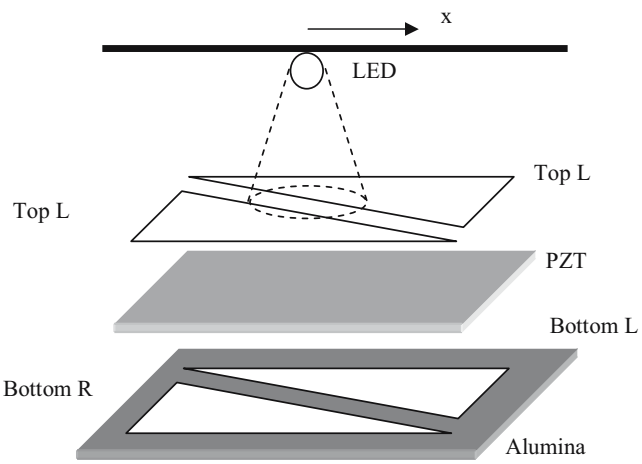

Fig. 19 Expanded view of pyroelectric displacement sensor (after Ferrari et al. [64])

9.1 Pyroelectric thick film sensors

Sensors have also been developed that exploit the pyroelectric effect of PZT thick-films. A displacement sensor based upon a moving LED and a fixed PZT pyroelectric sensor has been demonstrated by Ferrari et al. [64]. The pyroelectric

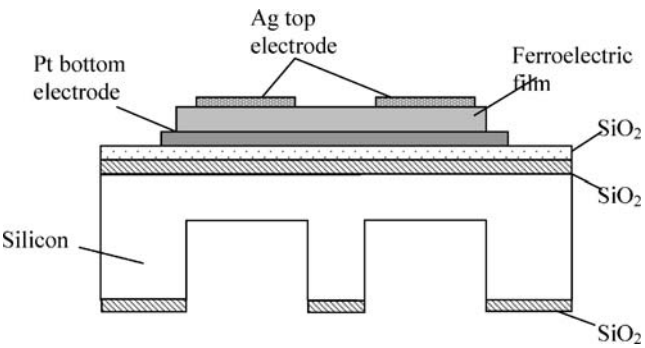

Fig. 20 Thick-film ferroelectric silicon actuator

response of the PZT layer is limited to a dynamic frequency response and therefore the source is modulated at 80 Hz. The sensor design uses a standard planar capacitor structure with four silver/palladium electrodes of triangular shape as shown in Fig. 19. The two pairs of electrodes are differentially poled and the output from one pair is subtracted from the other. At the central position (x=0) the net output is zero and this goes positive for movement to the right, negative for movement to the left. The differential poling arrangement also serves to cancel out the piezoelectric response of the sensor to mechanical vibrations. The pyroelectric coefficient of the PZT film was measured to be 1.4×10^{-4} cm^{-2} K^{-1}. The sensor achieved a displacement resolution of better than 0.15% of the measured span.

9.2 Thick-film actuators

Silicon micromachining techniques have also been applied to the fabrication of an array of actuators described by Futakuchi et al. [65]. The actuator structure, shown in Fig. 20, was first wet etched in KOH before processing the screen printed lower platinum electrode, ferroelectric film and silver top electrode. The ferroelectric film is composed of $Pb[Zr_{0.2}Ti_{0.3}(Mg_{1/3}Nb_{2/3})_{0.3}(Zn_{1/3}Nb_{2/3})_{0.1}-(Mg_{1/2}W_{1/2})_{0.1}]0_3$. The actuator membrane has an area of 3×10 mm^2 and the maximum displacement equalled approximately 0.5 μm for an applied voltage of 30 V and a membrane thickness of 100 μm.

10 Conclusions and future possibilities

This paper has demonstrated how thick-film technology can be used to fabricate a wide variety of piezoelectric devices. Many different examples of thick-film sensors and actuators have been described. A wide variety of substrate materials can be used for the devices including ceramics, stainless steels and silicon. In the latter case, it has also been shown that thick-film piezoelectrics can be used as a key element in MicroElectroMechanical Systems (MEMS). One of the drawbacks of the technology is that the minimum resolution of screen printed films is around 200 μm. Several research groups are currently studying ways to improve the resolution to allow improved compatibility with all aspects of MEMS processing.

References

1. N.M. White, J.D. Turner, Meas. Sci. Technol. **8**, 1–20 (1997)
2. J.E. Brignell, N.M. White, A.W.J Cranny, IEE Proc. I. **135**(4), 77–84 (1988)
3. H. Baudry, Proceedings of the sixth European Microelectronics Conference. 456–63 (1987)
4. B. Morten, G. De Cicco, M. Prudenziati, Proc. 7th European Hybrid Microelectronics Conference. paper 8.4 (1989)
5. B. Morten, G. De Cicco, A. Gandolfi, C. Tonelli, Proc. 8th European Hybrid Microelectronics Conference. 392–399 (1991)
6. H. Moilanen, S. Leppavuori, A. Uusimaki, Sens. Actuators A. **37–38**, 106–111 (1993)
7. E.S. Thiele, N. Setter, J. Am. Ceram. Soc. **83**, 1407–1412 (2000)
8. Take-Control Piezometer: http://www.take-control.demon.co.uk
9. J.E. Southin, S.A. Wilson, D. Schmitt, R.W. Whatmore, J. Phys. D: Appl. Phys. **34**, 1456–1460 (2001)
10. R.A. Dorey, R.W. Whatmore, Integr. Ferroelectr. **50**, 111–119 (2002)
11. R.N. Torah, S.P. Beeby, N.M. White, Sens. Actuators A. **110**(1–3), 378–384 (2004)
12. R.N. Torah, S.P. Beeby, N.M. White, IEEE Trans. Ultrason. Ferroelectr. Freq. Control **52**(1), 10–16 (2005)
13. G. Harsanyi, Sens. Rev. **20**, 98–105 (2000)
14. W.W. Clegg, D.F.L. Jenkins, M.J. Cunningham, Sens. Actuators A. **58**, 173–177 (1997)
15. P. Uebershlag, Sens. Rev. **21**, 118–125 (2001)
16. T. Papakostas, N.R. Harris, S.P. Beeby, N.M. White, Eurosensors XII Southampton 461–464 (1998)
17. R.N. Torah, S.P. Beeby, N.M. White, J. Appl. Phys. **37**, 1–5 (2004)
18. S.P. Beeby, N.M. White, Sens. Actuators A. **88**, 189–197 (2001)
19. T. Futakuchi, H. Yamano, M. Adachi, Jpn. J. Appl. Phys. **40**, 5687–5689 (2001)
20. J. Dargahi, Sens. Actuators A. **80**, 23–30 (2000)
21. R. Maas, M. Koch, N. Harris, N.M. White, A. Evans, Mater. Lett. **31**, 109–112 (1997)
22. H.D. Chen, K.R. Udayakumar, L.E. Cross, J. Appl. Phys. **77**, 3349–3353 (1995)
23. A. Kohler, P. Dullenkopf, Microelectron. Int. **17/3**, 7–10 (2000)
24. N.M. White, P. Glynne-Jones, S.P. Beeby, M.J. Tudor, M. Hill, Meas. Control **34**(9), 267–271 (2001)
25. N.M. White, P. Glynne-Jones, S.P. Beeby, Smart Mater. Struc. **10** (4), 1850–1852 (2001)
26. T. Yan, B.E. Jones, R.T. Rakowski, M.J. Tudor, S.P. Beeby, N.M White, IEE Electronics Letters **39**(13), 982–983 (2003)
27. Ultrasonic & Acoustic Transducer Group: Production of Piezoceramics, UK, Morgan Electro Ceramics Internal Publication
28. C. Robertson, R.D. Shipton, D.R. Gray, Sens. Rev. **19**(1), 33–36 (1999)
29. Sol Gel process website: http://www.chemat.com/html/solgel.html
30. Y.B. Kim, T.S. Kim, K.S. Choi, D.J. Choi, Integr. Ferroelectr. **35**, 199–208 (2001)
31. D.L. Corker, Q. Zhang, R.W. Whatmore, C. Perrin, J. Eur. Ceram. Soc. **22**, 383–390 (2002)
32. J. Dudek, Z. Wrobel, Ferroelectrics **18**, 161–164 (1978)
33. C.A. Randall, N. Kim, J.-P. Kucera, W. Cao, T.R. Shrout, J. Am. Ceram. Soc. **81**(3), 677–688 (1998)
34. P. Glynne-Jones, S.P. Beeby, P.G. Dargie, T.P. Papakostas, N.M. White, Meas. Sci. Technol. **11**, 526–531 (2000)
35. S.P. Beeby, A. Blackburn, N.M. White, Mater. Lett. **40**, 187–191 (1999)
36. S.P. Beeby, A. Blackburn, N.M. White, J. Micromechanics Microengineering **9**, 218–229 (1999)
37. E.S. Thiele, D. Damjanovic, N. Setter, J. Am. Ceram. Soc. **84**(12), 2863–2868 (2001)
38. M. Koch, N.R. Harris, R. Maas, A.G.R. Evans, N.M. White, A. Brunnschweiler, Meas. Sci. Technol. **8**, 49–57 (1997)
39. M. Koch, N.R. Harris, A.G.R. Evans, N.M. White, A. Brunnschweiler, Sens. Actuators A **A70**(1–2), 98–103 (1998)
40. K. Junwu, Y. Zhigang, R. Taijiang, C. Guangming, W. Boda, Sens. Actuators A **121**, 156–161 (2005)
41. Y.B. Kim, H.J. Kim, C.I. Cheon, D.J. Choi, T.S. Kim, Integr. Ferroelectr. **50**, 61–70 (2001)

42. D. Crescini, D. Marioli, E. Sardini, A. Taroni, Sens. Actuators A **87**, 131–138 (2001)
43. S.P. Beeby, J.N. Ross, N.M. White, IEE Electronics Letters **35** (23), 2060–2062 (1999)
44. M. Kurosawa, H. Inagaki, T. Higuchi, Ultrasonics **34**, 271–274 (1996)
45. T. Morita, M. Kurosawa, T. Higuchi, IEEE Trans. Ultrason. Ferroelectr. Freq. Control **45**(5), 1178–1186 (1998)
46. M. Hu, H. Du, F.S. Ling, J.K. Teo, Sens. Actuators A **94**, 113–116 (2001)
47. M. Aoyagi, S.P. Beeby, N.M. White, IEEE Trans. Ultrason. Ferroelectr. Freq. Control **49**(2), 151–158 (2002)
48. C.M. Light, P.H. Chappell, Med. Eng. Phys. **22**, 679–684 (2000)
49. A.W.J. Cranny, P.H. Chappell, S.P. Beeby, N.M. White, Proc. Eurosensors XVII. (Portugal 2003)
50. S.P. Beeby, N.M. White, Electron. Lett. **36**(19), 1661–1662 (2000)
51. S.P. Beeby, N.M. White, Sens. Actuators A **88**, 189–197 (2001)
52. V. Ferrari, D. Marioli, A. Taroni, Electron. Lett. **32**(9), 855–856 (1996)
53. V. Ferrari, D. Marioli, A. Taroni, Meas. Sci. Technol. **8**, 42–48 (1997)
54. H.J. Kim, Y.B. Kim, J.Y. Kang, T.S. Kim, Integr. Ferroelectr. **50**, 11–20 (2002)
55. B. Morten, G. De Cicco, M. Prudenziati, Sens. Actuators **41–42**, 33–38, (1994)
56. N.M. White, G.R. Leach, IEE Proc., Sci. Meas. Technol. **42**, 249–254 (1995)
57. N.M. White, V.T.K. Ko, Electron. Lett. **29**, 1807–1808 (1993)
58. J. Hale, T. Dyakowski, A. Jaworski, N.M. White, N. Harris, Proc. of Sensors and their Applications XII. 71–76 (Limerick 2003)
59. T. Dyakowski, J. Hale, N. Harris, A. Jaworski, A. Nowakowski, N.M. White, Y. Zhang, 3rd World Congress in Industrial Process Tomography. (Alberta 2003)
60. N. Harris, M. Hill, Y. Shen, R. Townsend, S.P. Beeby, N.M. White, Ultrasonics **42**, 139–144 (2004)
61. M. Hill, N. Harris, R. Townsend, N.M. White, S.P. Beeby, World Congress on Ultrasonics. (Paris 2003) 1647–1650
62. N.R. Harris, M. Hill, S. Beeby, Y. Shen, N.M. White, J.J. Hawkes, W.T. Coakley, Sens. Actuators B **95**, 425–434 (2003)
63. N.R. Harris, M. Hill, R. Torah, R. Townsend, S. Beeby, N.M. White, J. Ding, Proc. Of Eurosensors XIX. (Barcelona, 2005)
64. V. Ferrari, D. Marioli, A. Taroni, IEEE Trans. Instrum. Meas. **51** (4), 819–823 (2002)
65. T. Futakuchi, H. Yamano, M. Adachi, Jpn. J. Appl. Phys. **40**, 5687–5689 (2001)